Platinum-group mineralogy of the Giant Mascot Ni-Cu-PGE deposit, Hope, B.C.

Matthew J. Manor[1, a], James S. Scoates[1], Graham T. Nixon[2], and Doreen E. Ames[3]

[1] Pacific Centre for Isotopic and Geochemical Research, Department of Earth, Ocean and Atmospheric Sciences, University of British Columbia, Vancouver, BC, V6T 1Z4
[2] British Columbia Geological Survey, Ministry of Energy and Mines, Victoria, BC, V8W 9N3
[3] Geological Survey of Canada, Natural Resources Canada, 601 Booth St., Ottawa, ON, K1A 0E8
[a] corresponding author: mmanor@eos.ubc.ca

Recommended citation: Manor, M.J., Scoates, J.S., Nixon, G.T., and Ames, D.E., 2014. Platinum-group mineralogy of the Giant Mascot Ni-Cu-PGE deposit, Hope, B.C. In: Geological Fieldwork 2013, British Columbia Ministry of Energy and Mines, British Columbia Geological Survey Paper 2014-1, pp. 141-156.

Abstract

The Giant Mascot Ni-Cu-PGE deposit is British Columbia's only past-producing nickel mine (1958-1974), having yielded ~ 4.2 Mt of ore grading 0.77% Ni and 0.34% Cu with minor Co, Ag and Au. Intrusive ultramafic rocks (olivine-orthopyroxene ± hornblende ± clinopyroxene cumulates) host the Ni-Cu sulphide mineralization. Field mapping and petrographic study have revealed primary magmatic cumulus textures and minimal alteration of the ultramafic rocks. Platinum-group minerals (PGM) determined by microbeam techniques are predominantly bismuthotellurides, primarily moncheite [$(Pt,Pd)(Te,Bi)_2$], merenskyite [$Pd(Te,Bi)_2$], and palladian melonite [$(Ni,Pd)(Te,Bi)_2$]. Other precious-metal minerals include sperrylite ($PtAs_2$), hessite (Ag_2Te) and altaite (PbTe). Pt-, Pd- and Ni-bismuthotellurides are in or at the margins of base metal sulphides, predominantly pentlandite, or in fractures; precious-metal minerals are mostly along fractures in silicate minerals. Textures are consistent with an orthomagmatic origin for sulphides and PGM involving exsolution from base metal sulphides during cooling. Locally abundant fractures filled by chalcopyrite and platinum-rich moncheite are evidence for relatively late-stage mobilization of residual Cu-rich sulphide melts. PGE-enriched sulphides containing identifiable PGM and associated precious-metal minerals in the Giant Mascot intrusion indicate that 'orogenic' Ni-Cu mineralization in the Canadian Cordillera and elsewhere may provide significant exploration targets for economic Ni-Cu-PGE deposits.

Keywords: Giant Mascot, platinum-group minerals, Ni-Cu-PGE mineralization, ultramafic, magmatic sulphide, Coast Plutonic Complex, Spuzzum pluton

1. Introduction

Conventionally, subduction-zone environments are considered poor targets for nickel-copper-platinum group element (Ni-Cu-PGE) sulphide mineralization due to the paucity of ultramafic bodies with economic Ni-sulphides (Ripley, 2010). Although PGE mineralization in supra-subduction zone ('orogenic') settings is commonly associated with Ural-Alaskan-type intrusions (ultramafic bodies typically devoid of orthopyroxene), their prospectivity with respect to Ni-sulphides remains unclear (Nixon et al., 1997; Ripley, 2010). Nonetheless, Ni-Cu-PGE deposits in orogenic settings hosted by ultramafic-mafic rocks containing orthopyroxene as an essential mineral are becoming an increasingly important resource or exploration target (e.g., Aguablanca, Spain, Piña et al, 2008; Portneuf-Mauricie Domain, Québec, Sappin et al, 2012; St. Stephen, New Brunswick, Paktunc, 1989; Americano do Brasil and Limoeiro, Brazil, Mota-e-Silva et al., 2011, 2013).

To better understand these orogenic deposits, herein we present preliminary results from an ongoing study of the Giant Mascot Ni-Cu-PGE deposit in southern British Columbia (Fig. 1), where intrusive ultramafic rocks (olivine-orthopyroxene ± hornblende ± clinopyroxene cumulates) host Ni-Cu sulphide mineralization. Through field mapping, petrographic study, scanning electron microscopy, and electron microprobe analyses we provide the first systematic documentation of the occurrence and textural features of platinum-group minerals (PGM) and Ni-Cu sulphide mineralization hosted by the Giant Mascot intrusion.

2. Geological setting

The Giant Mascot deposit is east of Harrison Lake, approximately 12 kilometres north of Hope, in southwestern British Columbia. The deposit is in the Northern Cascade region near the southeastern margin of the Coast Plutonic Complex (Fig. 1; Brown and McClellan, 2000; Reiners et al., 2002). Plutons and batholiths in this area are catazonal to epizonal, tonalitic to gabbroic intrusions that were emplaced in a magmatic arc setting during the Cretaceous (107-76 Ma, Richards, 1971; Brown and McClellan, 2000; Mitrovic, 2013, and references therein).

The Spuzzum pluton (early Late Cretaceous, ca. 95 Ma, M.J. Manor, unpublished data), a 60 x 20 km granitoid batholith, hosts the Giant Mascot Ni-Cu-PGE deposit and associated ultramafic rocks (Fig. 1). It is compositionally zoned from pyroxene diorite in the core to hornblende diorite near the margins, and has an outermost rim of tonalite (Richards and McTaggart, 1976; Vining, 1977). The pluton intrudes Settler schist (Upper Triassic), a Barrovian-facies metamorphic complex consisting of pelitic and quartzofeldspathic schist and micaceous quartzite, and locally containing garnet, staurolite and kyanite (Pigage, 1973; Mitrovic, 2013).

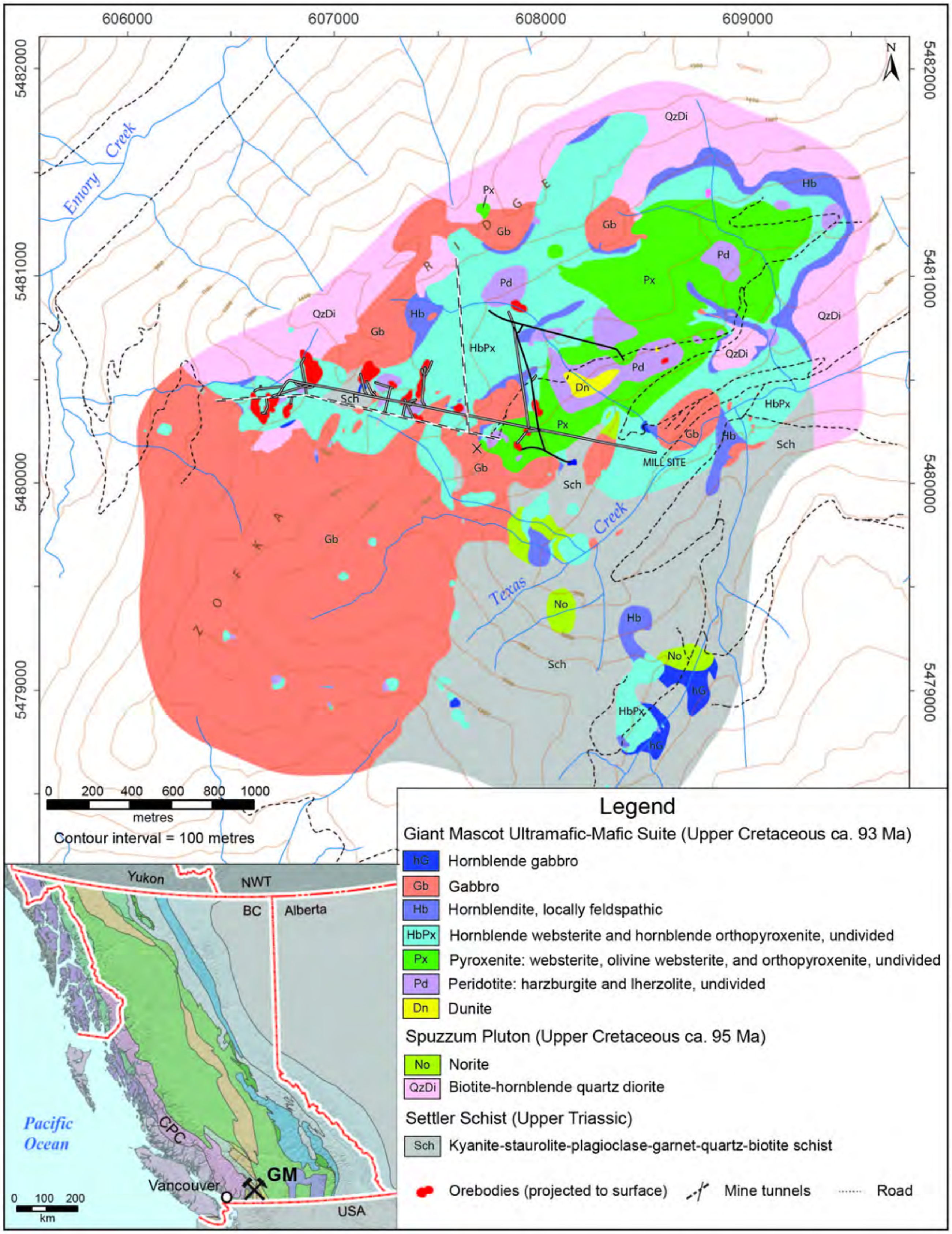

Fig. 1. Geologic map of the Giant Mascot ultramafic-mafic intrusion (modified from Aho, 1954) and inset showing its location in southwestern British Columbia (GM, Giant Mascot; CPC, Coast Plutonic Complex). The cross at map centre marks UTM coordinates of 607700 E, 5480180 N (NAD83, Zone 10).

3. Giant Mascot mine history

The Giant Mascot Ni-Cu-PGE deposit is British Columbia's only past-producing nickel mine (Pinsent, 2002). Nickel showings were first discovered in 1923, and diamond drilling defined the orebodies up until 1937. After a hiatus during and after World War II, exploration resumed in 1951, and the mine went into production in 1958 (Fig. 2). The deposit was mined for nickel and copper from 1958 to 1974 by open-stope methods, and produced approximately 4.2 Mt of ore with average grades of 0.77% Ni and 0.34% Cu along with minor Co, Ag and Au (Christopher and Robinson, 1974). Platinum-group-element abundances in the ores of the Giant Mascot deposit were uncertain or unreported (Pinsent, 2002; Nixon, 2003). Metcalfe et al. (2002) reported "platinum values in excess of 1 gram," although a specific source was not cited, and Hulbert (2001) reported six PGE analyses without any geologic or mineralogic information.

Fig. 2. Photograph from Western Miner (Stephens, 1959) showing the main mill site at Giant Mascot in the early years of production and the primary crusher (centre) and secondary crusher (left).

A total of 28 orebodies occur along a west-east mineralized corridor (orebodies projected to surface, Fig. 1). Twenty-two of these were mined, including five major contributors to production: Pride of Emory, Brunswick #2 and #5, 4600, and 1500 (Christopher and Robinson, 1974). Mine workings and major portals to the underground stopes are north of Texas Creek, on the southern slope of Zofka Ridge (Fig. 1).

4. Lithological units

The Giant Mascot intrusion, a crudely elliptical, 4 x 3 km body, comprises ultramafic and mafic rocks that are hosted by quartz diorites of the Spuzzum pluton and metapelites of the Settler schist (Fig. 1). Nine main rock units (Figs. 1, 3) include ultramafic, mafic and country-rock lithologies, where each lithology is characterized by a range of mineral compositions. Mean olivine, pyroxene, and plagioclase compositions determined by electron microprobe analysis (EMPA) are reported in Muir (1971) and McLeod (1975). In addition, plagioclase compositions (n=19) for gabbro and quartz diorite have been determined optically in this study based on the Michel-Levy method.

4.1. Ultramafic rocks

The Giant Mascot ultramafic-mafic intrusion (ca. 93 Ma; M.J. Manor, unpublished data) consists predominantly of olivine- and orthopyroxene-rich cumulates with variable amounts of clinopyroxene and hornblende. The rocks display primary igneous textures involving olivine, orthopyroxene, clinopyroxene, and hornblende, with minor biotite, plagioclase, and quartz. Minor secondary alteration occurs mostly at grain boundaries as tremolite-actinolite, chromian Mg-chlorite, talc, serpentine, and carbonate. Alteration of clinopyroxene to hornblende is common, whereas reaction of orthopyroxene to hornblende is less prevalent.

The major ultramafic units are dunite, peridotite and pyroxenite; the latter two lithologies contain variable amounts of hornblende. Dunite occurs in the core of the intrusion and, although the smallest rock unit by volume, is a major host of nickel mineralization. The rock is fine grained and contains 90-95 vol.% equigranular olivine with sparse euhedral chromite inclusions and secondary Cr-magnetite, interstitial clinopyroxene (5-10%), and minor orthopyroxene. Peridotite, the other major host of mineralization, is represented by fine- to medium-grained lherzolite and harzburgite orthocumulates with variable amounts of hornblende. Olivine (40-80%; ~Fo_{84}; Muir, 1971) occurs as cumulus crystals or grains enclosed in subpoikilitic pyroxene. Intergranular orthopyroxene (30-60%) is the predominant pyroxene (En_{84}; Muir, 1971), accompanied by variable (0-10%) clinopyroxene and interstitial hornblende. Pyroxenite typically contains no sulphide and forms medium-grained orthocumulates of websterite, olivine websterite, and orthopyroxenite. Brown subhedral orthopyroxene (En_{82}; Muir, 1971) forms sparse oikocrysts and is more abundant than black-green clinopyroxene (55-90% total pyroxene). Olivine (5-35%) forms intergranular grains or inclusions, whereas hornblende (0-10%) is interstitial. Locally, plagioclase (5-10%) occurs in clots.

Hornblende-rich units of the Giant Mascot ultramafic-mafic intrusion include hornblende pyroxenite and hornblendite. Hornblende pyroxenites are medium-grained hornblende websterite and orthopyroxenite, commonly oikocrystic and locally feldspathic. Orthopyroxene (En_{77-81}; Muir, 1971) and clinopyroxene abundances are highly variable (20-60%) and textures are predominantly cumulate. Pyroxene grains are commonly enclosed by oikocrystic hornblende (20-80%), which ranges in diameter from 4 to 50 mm. Hornblendite commonly occurs at marginal contacts with gabbro and Spuzzum quartz diorite, where it typically forms feldspathic pegmatite zones up to 40 m wide at the contact. Prismatic hornblende (90-98%) ranges in length from 0.2 to 25 cm and is commonly altered to cummingtonite-tremolite intergrowths and anthophyllite. Clinopyroxene (0-5%) is interstitial or forms euhedral inclusions in pegmatitic hornblende. Locally, plagioclase clots (An_{80-90}; McLeod, 1975) may attain 30% of the mode. Hornblende pyroxenite rarely contains sulphide; exceptions are reported in the Chinaman, Climax and 4300 orebodies, which hosted disseminated and minor massive sulphide mineralization (Christopher and Robinson, 1974).

4.2. Mafic rocks

Hornblende gabbro is a minor lithology in the Giant Mascot intrusion. It is medium to coarse grained and variably

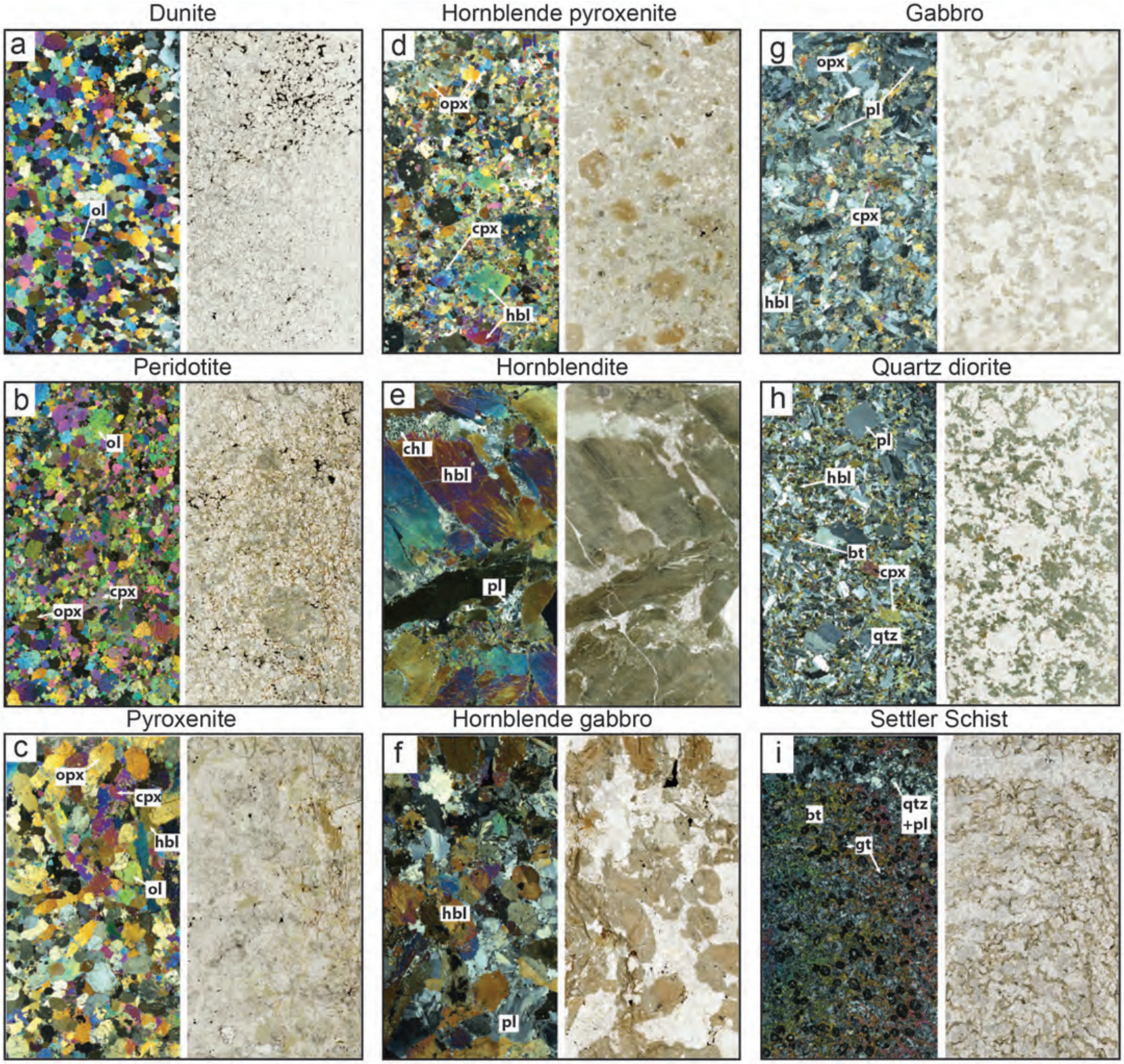

Fig. 3. Scanned images of thin sections showing lithological units at the Giant Mascot intrusion. Ultramafic units: **a)** dunite, sample 12MMA-7-8-1; **b)** peridotite, 12MMA-7-10-1; **c)** pyroxenite, 12MMA-5-4-1; **d)** hornblende pyroxenite, 12MMA-2-4-1; **e)** hornblendite, 11GNX-1-2-1. Mafic units: **f)** hornblende gabbro, 13MMA-9-9-3; **g)** gabbro, 12MMA-9-1-2. Country rocks: **h)** Spuzzum quartz diorite, 12MMA-2-1-5; **i)** Settler schist, 13MMA-5-1-1. Cross-polarized (left) and plain-polarized light (right) thin sections are 2 x 4 cm. Mineral abbreviations: ol, olivine; opx, orthopyroxene; cpx, clinopyroxene; hbl, hornblende; bt, biotite; pl, plagioclase; chl, chlorite; qtz, quartz; gt, garnet.

melanocratic, and contains subhedral, prismatic hornblende (15-55%), interstitial plagioclase (30-75%), and interstitial pyroxene (5-15%). Veins and dikes of unmineralized hornblende gabbro, one of the youngest intrusive phases, cut all mafic and ultramafic units.

Two-pyroxene gabbro is common along the margins of the intrusion, or within ultramafic rocks, and contains plagioclase (An_{48-72}; 45-70%), orthopyroxene and clinopyroxene (15-35%), hornblende (5-15%), biotite (0-5%), and quartz (0-15%). These gabbros share many mineralogical similarities to dioritic units in the surrounding Spuzzum pluton. Locally, gabbro intruding hornblende pyroxenite and Spuzzum quartz diorite displays chilled margins, and the gabbro contains rare lobate hornblende pyroxenite inclusions.

Norite units were mapped by Aho (1954, 1956) as orthopyroxene-plagioclase rocks (An_{65-90}; McLeod, 1975) that define small pods in contact with Settler schist. Our field and petrographic observations revealed significant clinopyroxene in these noritic units, which thus appear similar in composition to the gabbroic units described above.

The youngest phases of the Giant Mascot intrusion are felsic pegmatite and aplite veins and dikes (2-10 cm wide) cutting hornblendite, hornblende pyroxenite, hornblende gabbro, and gabbro.

4.3. Country rocks

The Spuzzum pluton, comprising diorite, quartz diorite, and tonalite, hosts the Giant Mascot ultramafic-mafic intrusion. Adjacent to the ultramafic rocks are white to grey, variably melanocratic, medium-grained, hornblende-biotite quartz diorite and diorite (An_{32-55}). Locally, these rocks are foliated; foliation is particularly well developed at pluton contacts. The main (15-55%) components of these diorites are orthopyroxene, clinopyroxene, hornblende, and biotite (± phlogopite). The diorites contain local lobate and elongate melanocratic inclusions rich in hornblende and biotite (> 90% mafic minerals).

The Settler schist is a series of layered metasedimentary rocks (siltstones and quartzofeldspathic arenites) that crop out on the east and southeast margins of the intrusion (Fig. 1). Schist directly in contact with the Giant Mascot intrusion contains variable proportions of kyanite, staurolite, and garnet, and strongly foliated biotite, quartz, and plagioclase. In the western part of Zofka Ridge, a large raft of Settler schist is in contact with hornblende pyroxenite to the west and gabbro on all other sides. At its northern contact, the schist locally exhibits evidence of incipient anatectic melting adjacent to a 70 x 100 m zone of garnetiferous gabbro that is cut by siliceous veins (Fig. 1).

5. Ni-Cu-PGE mineralization

Ni-Cu-PGE sulphide mineralization in the Giant Mascot intrusion is commonly hosted in the olivine-rich rocks, including dunite, peridotite, and olivine-bearing pyroxenite. Sulphide orebodies occur in 28 steeply dipping, north-northwest-trending, pipe-like structures that have diameters of 6 to 75 m and extend to depths of 30 to 360 m (Christopher and Robinson, 1974). At both outcrop and hand-sample scale, mineralization defines disseminated, net-textured, semi-massive and massive textures, and locally forms Cu-rich veins (Figs. 4a-h). Polished ore samples reveal brecciated textures in which olivine and pyroxene cumulates form inclusions in sulphide (Fig. 4e), or discontinuous intrastratal folds interpreted to record syndepositional ductile deformation during emplacement of the orebodies (Fig. 4g).

5.1. Mineralogy

The predominant sulphide minerals, present in all ores of the Giant Mascot intrusion, are pyrrhotite ($Fe_{1-x}S$), pentlandite [$(Fe,Ni)_9S_8$], chalcopyrite ($CuFeS_2$), and minor pyrite (FeS_2). Pyrrhotite is the most abundant sulphide (Fig. 4), both as magnetic, monoclinic (Fe_7S_8), and non-magnetic, hexagonal (e.g., $Fe_{11}S_{12}$), varieties (e.g., Becker et al., 2010). Pyrrhotite and pentlandite were the first sulphide minerals to crystallize from the sulphide melt, with chalcopyrite and pyrite following at somewhat lower temperatures (based on Naldrett, 2004). Minor phases include troilite (pure FeS), magnetite, argentopentlandite [$Ag(Fe,Ni)_8S_8$], mackinawite [$(Fe,Ni)_{1+x}S$], cubanite (Cu_3FeS_4), cobaltite (CoAsS), gersdorffite (NiAsS), and nickeline (NiAs). Sulphide phases associated with secondary alteration include pyrite, marcasite, violarite ($FeNi_2S_4$), and polydymite ($Ni^{2+}Ni^{3+}{}_2S_4$).

5.2. Sulphide textures

Pyrrhotite, the predominant sulphide, is commonly massive, and locally infills fractures in silicate minerals. Pentlandite may be massive and blocky (Figs. 5a, c, d, h) or form crystallographically oriented exsolution lamellae in pyrrhotite and argentopentlandite (Figs. 5b, c, g). The pyrrhotite:pentlandite ratio is approximately 2:1. Chalcopyrite is typically massive (Figs. 5a, d, f, g, i) or fills fractures in silicate minerals and pyrrhotite (Fig. 5e). Pyrite-pentlandite and pyrite-chalcopyrite symplectic intergrowths surround blocky pentlandite (Fig. 5a). Argentopentlandite is invariably found with chalcopyrite as exsolution lamellae and euhedral grains. Locally, pentlandite exsolved at crystallographic orientations in argentopentlandite (Figs. 5g; 6h). Low-temperature exsolution lamellae are common features in pentlandite, troilite, mackinawite and cubanite. Troilite is locally massive, but more commonly defines exsolution lamellae hosted by pyrrhotite (Fig. 5b). Mackinawite and cubanite form exsolution lamellae in pentlandite (Fig. 5h) and chalcopyrite (Fig. 5i), respectively.

Sulpharsenide minerals, such as gersdorffite, cobaltite and nickeline, are euhedral to subhedral grains hosting or contacting PGM or precious-metal minerals (PMM) (Figs. 6f, i). Secondary sulphides include marcasite, which occurs as veins within pyrrhotite (Fig. 5e), and pyrite, common as veins in pyrrhotite and pentlandite (Figs. 5d, e). Magnetite forms both euhedral inclusions in pyrrhotite or veins cutting pyrrhotite and chalcopyrite (Fig. 5f).

6. Microbeam techniques

6.1. Scanning electron microscopy (SEM)

Polished petrographic thin sections (n=10) were carbon coated and prepared in the Electron Microbeam/X-Ray Diffraction Facility at the University of British Columbia, Vancouver (UBC) and the SEM Facility at the Geological Survey of Canada, Ottawa (GSC). At UBC, back-scattered electron (BSE) imaging and qualitative energy-dispersive spectrometry (EDS) were carried out on a Philips XL-30 scanning electron microscope (SEM) equipped with a Bruker Quanta 200 energy-dispersion X-ray microanalysis system. An operating voltage of 15 kV was used, with a spot diameter of 6 µm and peak count time of 30 s. At the GSC, BSE imaging and EDS analyses were carried out on a Zeiss EVO 50 series SEM with extended pressure capability (up to 3000 Pascals), and equipped with a backscattered electron detector (BSD), Everhart-Thornley secondary electron detector (SE) and variable pressure secondary electron detector (VPSE). The Oxford EDS system includes the X-MAX 150 Silicon Drift Detector, INCA Energy 450 software and Aztec microanalysis software. An operating voltage (EHT) of 20 kV was used, with a probe current of 400 pA to 1 nA and peak count time of 30 s.

6.2. Electron microprobe analysis (EMPA)

Quantitative mineral analyses on PGM were carried out on carbon-coated, polished petrographic thin sections (n=9) using an automated four-spectrometer Cameca Camebax MBX electron microprobe by wavelength-dispersive X-ray analysis (WDX) at the Department of Earth Sciences, Carleton

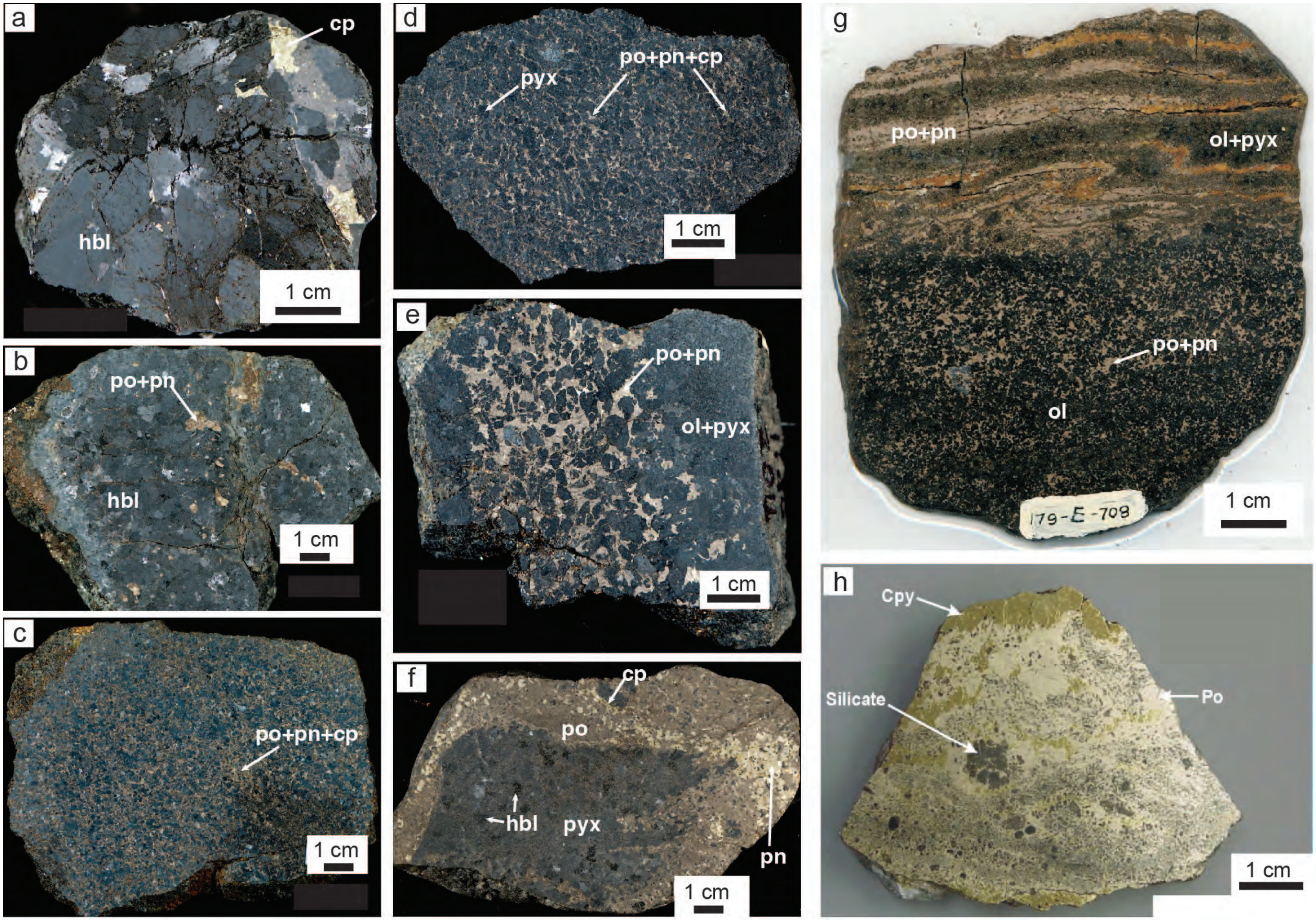

Fig. 4. Photographs of samples showing the range of mineralization types found in the Giant Mascot intrusion. **a)** 71-EI-624: hornblendite with chalcopyrite veins. **b)** 71-EI-622: disseminated pyrrhotite and pentlandite within hornblendite. **c)** 11AV-200: weakly net-textured pyrrhotite, pentlandite and chalcopyrite in pyroxenite. **d)** 11AV-201: moderately net-textured pyrrhotite, pentlandite and chalcopyrite in pyroxenite. **e)** 11AV-204: strongly net-textured pyrrhotite and pentlandite in peridotite. **f)** 71-EI-659: massive pyrrhotite, pentlandite and minor chalcopyrite in hornblende pyroxenite. **g)** 179-E-709: folded bands of disseminated pyrrhotite, pentlandite and olivine-rich peridotite at the contact with dunite. **h)** RHP01-076: massive pyrrhotite containing chalcopyrite veins and a rounded silicate inclusion. Mineral abbreviations: po, pyrrhotite; pn, pentlandite; cp/cpy, chalcopyrite; hbl, hornblende; pyx, pyroxene; ol, olivine.

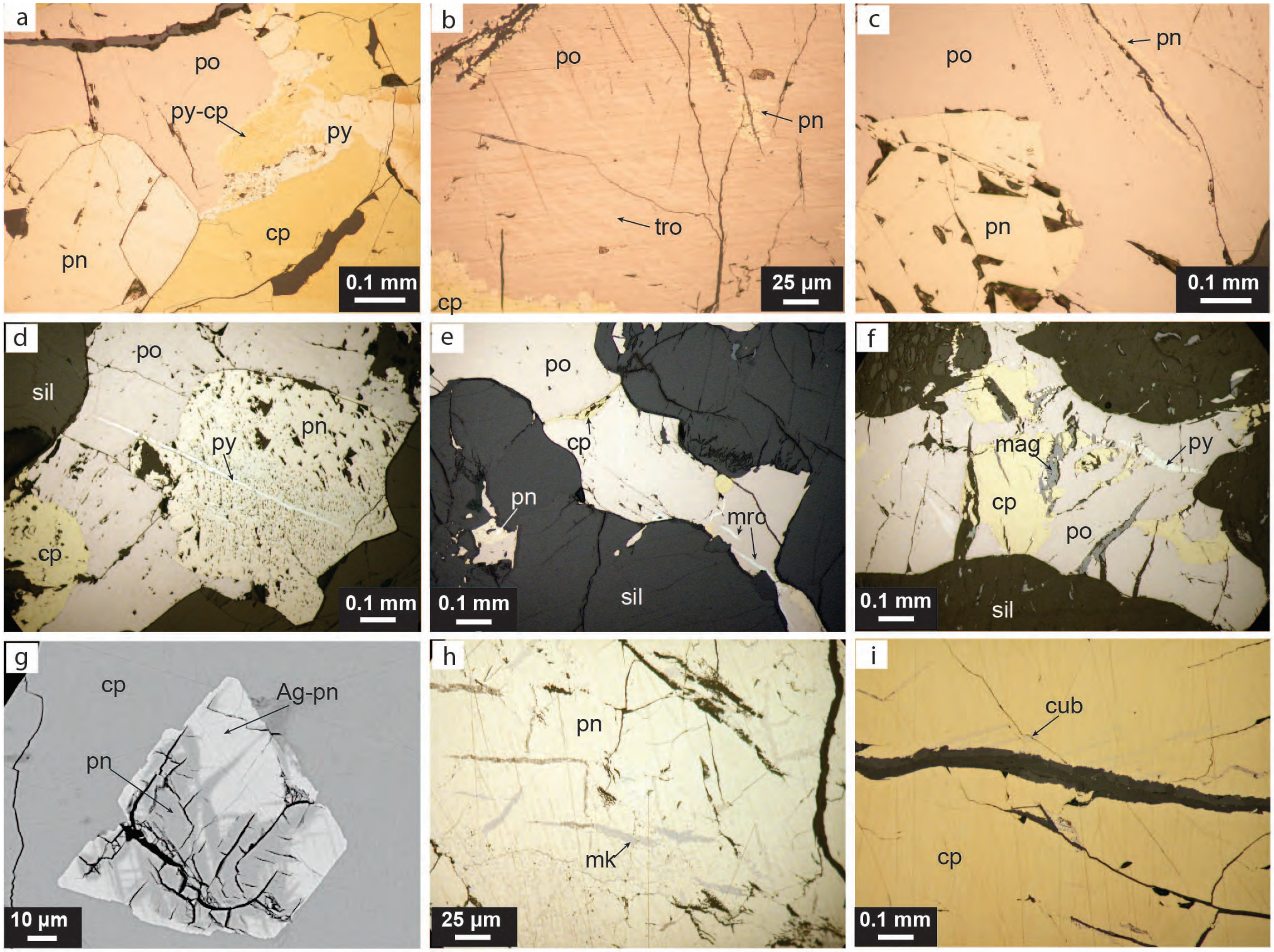

Fig. 5. Photomicrographs and backscatter electron (BSE) images of sulphide textures in the Giant Mascot intrusion. **a)** 71-EI-636: blocky pentlandite, massive chalcopyrite and pyrite, and symplectic chalcopyrite-pyrite hosted by massive pyrrhotite. **b)** 12MMA-5-8-5A: troilite exsolution lamellae, pentlandite flames and minor chalcopyrite in massive pyrrhotite. **c)** 71-EI-615C: two forms of pentlandite, blocky grains and exsolution lamellae, hosted by massive pyrrhotite. **d)** 71-EI-634: blocky pentlandite, pyrite-pentlandite intergrowths and chalcopyrite in pyrrhotite, with a pyrite vein cutting the intergrowths and pyrrhotite. **e)** 71-EI-636: net-textured pyrrhotite containing chalcopyrite veins and marcasite flames. **f)** M29-21: pyrrhotite and chalcopyrite containing veins of pyrite and magnetite. **g)** 71-EI-624A: argentopentlandite with pentlandite exsolution lamellae hosted by chalcopyrite (BSE). **h)** 12MMA-5-8-5A: massive pentlandite containing mackinawite [$(Fe,Ni)_{1+x}S$] exsolution lamellae. **i)** RHP01-078: massive chalcopyrite containing cubanite exsolution lamellae. Mineral abbreviations: po, pyrrhotite; pn, pentlandite; Ag-pn, argentopentlandite; cp, chalcopyrite; py, pyrite; tro, troilite; mrc, marcasite; mag, magnetite; mk, mackinawite; cub, cubanite; sil, silicate.

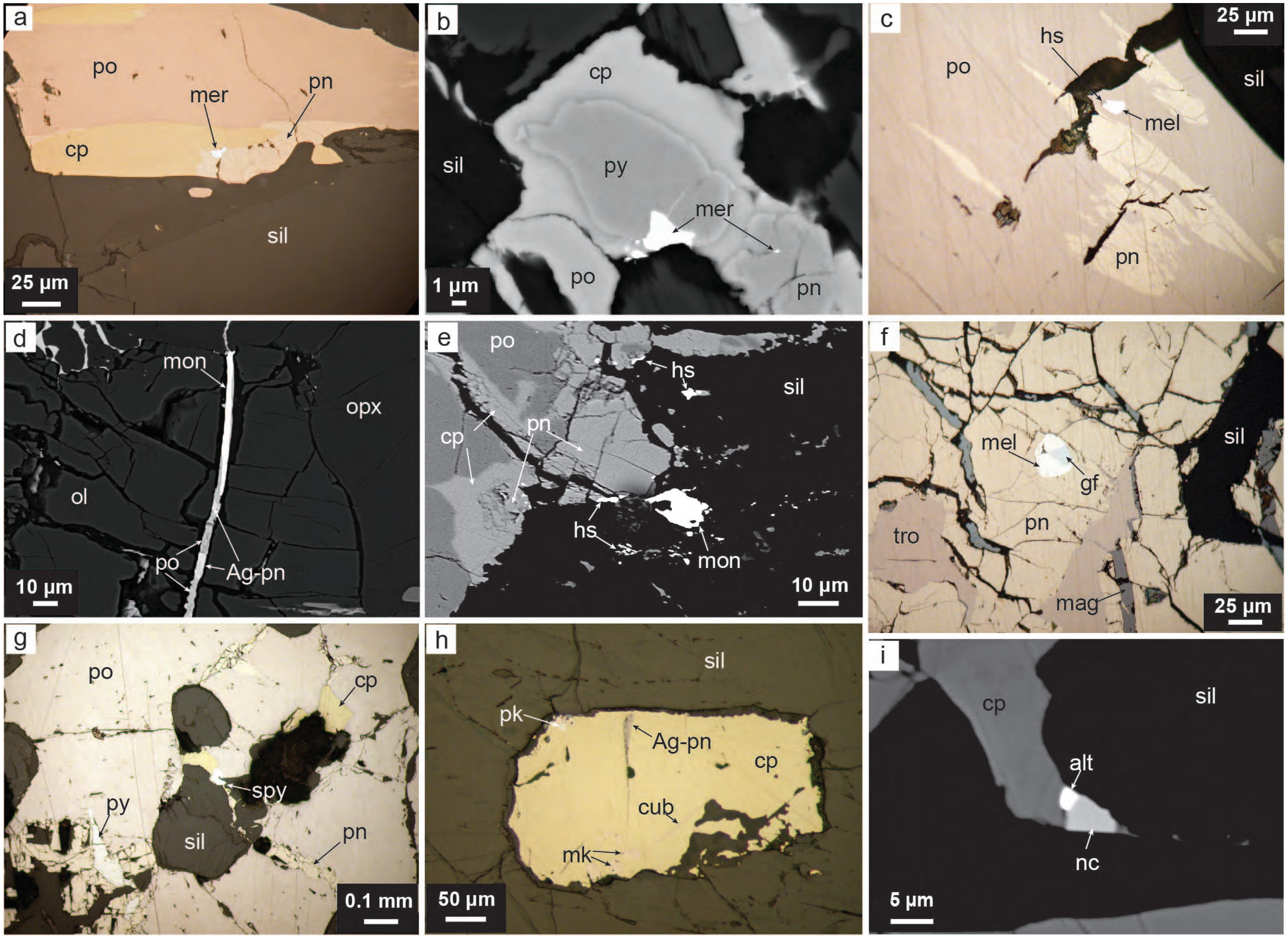

Fig. 6. Photomicrographs and backscatter electron (BSE) images of platinum-group and precious-metal minerals in Giant Mascot ores. **a)** 71-EI-615A: bright white anhedral merenskyite hosted by pentlandite at the grain boundary of chalcopyrite, both within pyrrhotite. **b)** 179-E-847: merenskyite hosted in pyrite and chalcopyrite, and associated with pyrrhotite and pentlandite (BSE); **c)** 12MMA-5-8-5A: bright white, anhedral palladian melonite tipped by hessite and fully enclosed in pyrrhotite proximal to pentlandite flames. **d)** RHP01-078: moncheite hosted by a chalcopyrite and argentopentlandite compound vein within fractured olivine (BSE). **e)** RHP01-152: moncheite fully enclosed by silicates, a smaller elongate moncheite at the boundary of pentlandite and silicate, and small satellite grains of hessite fully enclosed in silicates and along silicate-sulphide boundaries (BSE). **f)** 12MMA-5-8-5A: bright white, anhedral palladian melonite intergrown with euhedral gersdorffite, hosted by pentlandite containing magnetite veins, and surrounded by troilite. **g)** 71-EI-657: bright white sperrylite at the boundary of chalcopyrite and pyrrhotite, blocky pentlandite and pentlandite flames proximal to pyrite. **h)** RHP01-109: cream-coloured parkerite enclosed in chalcopyrite containing argentopentlandite, mackinawite and cubanite flames. **i)** RHP01-109: altaite in contact with chalcopyrite, nickeline, and silicates (BSE). Mineral abbreviations as in Figure 5 except: mer, merenskyite; mel, palladian melonite; mon, moncheite; hs, hessite; spy, sperrylite; pk, parkerite; alt, altaite; nc, nickeline; ger, gersdorffite; ol, olivine; opx, orthopyroxene.

University, Ottawa. Raw X-ray data were converted to elemental weight percent by the Cameca PAP matrix correction program. Tellurides and PMM were analyzed using a 20 keV accelerating voltage, 35 nA beam current, 2 µm diameter beam, and counting time of 10 seconds or 40,000 accumulated counts.

7. Results

7.1. PGM: Bismuthotellurides, bismuthides, and arsenides

Samples initially chosen for PGM analysis included those with high PGE abundances in whole rocks (> 1 ppm total PGE; M.J. Manor, unpublished data). Most of the PGM identified are tellurides or bismuthotellurides, predominantly merenskyite ($PdTe_2$), moncheite ($PtTe_2$) and melonite ($NiTe_2$) (Tables 1, 2). The PGM are most commonly associated with base metal sulphides (BMS), predominantly pentlandite (Figs. 6b, c; 7c). In addition, PGM may be either fully enclosed in sulphide, at sulphide-sulphide or sulphide-silicate interfaces, in sulphide veins in other sulphides or silicates, or as satellite grains in fractured silicates.

Merenskyite (3-23 µm) occurs in three compositional varieties: Pt-rich, Ni-rich, and near-stoichiometric merenskyite (28 total grains). Merenskyite grains are invariably associated with BMS (pyrrhotite, pentlandite, chalcopyrite, pyrite, troilite) and are either fully enclosed by sulphides or occur at sulphide-sulphide or sulphide-silicate interfaces (Figs. 6a, b).

Moncheite (2-56 µm) is the predominant telluride (30 total grains). Palladian moncheite has an average composition of $[(Pt_{0.35}Pd_{0.31})(Te_{1.87}Bi_{0.14})]$ (n=3). Grains are fully enclosed in pyrrhotite, pentlandite, chalcopyrite or silicate, or occur at sulphide-sulphide or sulphide-silicate interfaces. Moncheite is also common as inclusions in fracture-filling compound veins of chalcopyrite and argentopentlandite, with rare examples of < 160 µm long stringers (Figs. 6d, e).

A nickel-bearing telluride, palladian melonite (< 30 µm), has an average composition of $[(Ni_{0.84}Pd_{0.23})(Te_{1.87}Bi_{0.13})]$ (n=11). Grains of Pd-melonite invariably form inclusions in pyrrhotite, pentlandite and troilite (Figs. 6c, f).

Froodite ($PdBi_2$) is comparatively rare, and occurs as a satellite grain enclosed in silicate, but in contact with chalcopyrite. Sperrylite (< 50 µm), the only arsenide observed, has a nearly stoichiometric composition $[Pt_{0.80}As_{2.00}]$ (n=2). It is found either fully enclosed by chalcopyrite or at chalcopyrite-pyrrhotite-silicate interfaces (Fig. 6g).

7.2 Precious-metal minerals (PMM)

Hessite (Ag_2Te) is the most common PMM (> 75 grains) and occurs in cubanite, chalcopyrite, pentlandite, and silicate, at sulphide-sulphide or sulphide-silicate interfaces, or is intergrown with moncheite. It is most commonly found as satellite grains in fractures in silicate minerals (Figs. 6c, e). Hessite is typically in samples containing the highest concentrations of PGE. Rare altaite (PbTe) typically is associated with chalcopyrite (Fig. 6i). A single grain of hedleyite ($Bi_{2+x}Te_{1-x}$) was observed in silicate. Tellurobismuthite (Bi_2Te_3) is either fully enclosed by, or at the contacts between, pentlandite and pyrrhotite.

Parkerite ($Ni_3Bi_2S_2$) is a rare sulphobismuthide mineral. It is associated with chalcopyrite, locally at chalcopyrite-silicate interfaces (Fig. 6h). One grain of hollingworthite (RhAsS) as a composite grain with Ni-merenskyite was observed in a compound vein of chalcopyrite and pentlandite. Native Te and Bi grains are in pyrrhotite and pentlandite and at sulphide-silicate interfaces.

8. Discussion

Bismuthotellurides in the Giant Mascot Ni-Cu-PGE deposit exhibit a bimodal distribution between the $PtTe_2$ – $PdTe_2$ and $NiTe_2$ – $PdTe_2$ solid solution joins (Fig. 7a), forming a moncheite-merenskyite group and a merenskyite-melonite group. Analyses from the first group lie along the $PtTe_2$ – $PdTe_2$ join and most grains belong to the moncheite-merenskyite series. Tellurium contents vary substantially, such that Pt-rich merenskyite grains fall in the moncheite field, and all solid solutions are relatively Ni-poor. The second group on the $NiTe_2$ – $PdTe_2$ join contains the merenskyite-melonite series. Merenskyite is more abundant in this group compared to the $PtTe_2$ – $PdTe_2$ join, and relatively Pt-poor. The range of compositions is greater, and includes both Ni-rich merenskyite and palladian melonite. This bimodal distribution of Pt-Pd-Ni bismuthotellurides is also observed in sulphide ores from the Wellgreen Ni-Cu-PGE deposit in the northern Canadian Cordillera (Yukon) part of the Wrangellia large igneous province (Triassic; Greene et al., 2009). There, significant abundances of Sb- and As-rich PGM were reported by Barkov et al. (2002), whereas rare examples of arsenides are observed in the Giant Mascot intrusion (i.e., sperrylite). Platinum-group minerals in the Giant Mascot intrusion share features with minerals in the Aguablanca Ni-Cu-PGE deposit in Spain, notably the presence of palladian melonite-merenskyite-moncheite solid solutions. However, the Aguablanca ores contain higher abundances of Sb and Bi, allowing for the crystallization of the michnerite (PdBiTe) and the Sb-rich end-member testibiopalladite [Pd(Sb,Bi)Te] (Piña et al., 2008).

Precious-metal minerals in the Giant Mascot sulphide ores are rich in Ag, Pb, Ni, As, Bi, Te and S, but lack PGE. The presence of these elements, associated with chalcopyrite and located within fractures in primary silicates (i.e., olivine and pyroxene), is consistent with late-stage magmatic mobilization of a residual Cu- and semimetal-rich melt (Helmy, 2005). The residual melts from which the PMM crystallized were likely rich in base and precious metals relative to the original sulphide melt that crystallized Pt-, Pd- and Ni-bearing bismuthotellurides.

The textural characteristics of PGM in the Giant Mascot intrusion indicate two possible mechanisms of formation: 1) exsolution from primary BMS minerals at relatively high temperatures, either along crystallographic interfaces, at sulphide compositional boundaries, or by nucleation along fractures in sulphides (Figs. 7b, c; e.g., Cabri and Laflamme, 1976); or 2) formation of an immiscible PGE- and semimetal-rich melt for which components are incompatible in monosulphide solid solution (mss) and intermediate solid solution (iss) (650-250°C; Holwell and McDonald, 2010), the solid precursors to pyrrhotite and chalcopyrite, respectively. Locally abundant fractures filled by chalcopyrite and Pt-rich bismuthotellurides are evidence for relatively late-stage mobilization of Cu-rich residual sulphide melts. The predominance of various telluride minerals in the Giant Mascot intrusion (Fig. 7b) indicates a relatively high Te concentration in the parental magma. Tellurium may have been derived either directly from the arc mantle source or was introduced via crustal assimilation of metapelitic lithologies in the Settler schist (e.g., Afifi et al.,

Table 1. SEM energy-dispersive spectral analyses of platinum-group and precious-metal minerals from the Giant Mascot Ni-Cu-PGE deposit. SEM EDS analyses normalized to 100%.

				wt.%										
Sample name	Mineralization[1]	Host mineral[2]	Host rock[3]	Pt	Pd	Bi	Te	Ag	Ni	S	Pb	Rh	As	Mineral Name
3550 East Portal Dump														
RHP01-152-5-1	NT/HPGE	po/pn	ol websterite	21.0	9.9	10.9	58.3							merenskyite
RHP01-152-8-1	NT/HPGE	cp/sil	ol websterite	14.9	12.1	19.2	53.8							moncheite
RHP01-152-20-1	NT/HPGE	po/cp	ol websterite	30.4	8.3		61.3							Pt-merenskyite
RHP01-152-22-1	NT/HPGE	sil	ol websterite	33.0	4.4	8.8	53.8							moncheite
RHP01-152-22-2	NT/HPGE	sil	ol websterite				36.4	63.6						hessite
RHP01-152-22-3	NT/HPGE	sil	ol websterite				36.4	63.6						hessite
RHP01-152-22-4	NT/HPGE	cp/sil	ol websterite				36.4	63.6						hessite
RHP01-152-22-5	NT/HPGE	pn	ol websterite				36.4	63.6						hessite
RHP01-152-23-1	NT/HPGE	sil	ol websterite				37.4	62.6						hessite
RHP01-152-23-2	NT/HPGE	pn	ol websterite				37.4	62.6						hessite
RHP01-152-23-3	NT/HPGE	po	ol websterite	41.9			58.1							moncheite
RHP01-152-24-1	NT/HPGE	po/pn/sil	ol websterite	41.7			56.8	1.6						moncheite
RHP01-152-24-2	NT/HPGE	po/pn/sil	ol websterite	41.7			56.8	1.6						moncheite
RHP01-152-24-3	NT/HPGE	po/pn/sil	ol websterite	41.7			56.8	1.6						moncheite
RHP01-152-25-1	NT/HPGE	pn	ol websterite	10.6	16.8		72.6							merenskyite
RHP01-152-27-1	NT/HPGE	pn	ol websterite	22.8	7.1	6.4	63.8							moncheite
RHP01-152-28-1	NT/HPGE	pn/po	ol websterite	20.4	12.6		67.0							moncheite
RHP01-152-28-2	NT/HPGE	pn/po	ol websterite	20.4	12.6		67.0							moncheite
RHP01-152-28-3	NT/HPGE	pn/po	ol websterite	20.4	12.6		67.0							moncheite
12MMA-5-8-5A-1	CD	pn	lherzolite		12.5		87.5							merenskyite
12MMA-5-8-5A-2	CD	po	lherzolite		7.7	27.1	65.2							tellurobismuthite
RHP01-078-1	CD/HPGE	cp	hbl harzburgite	20.9	11.1		68.0							moncheite
RHP01-078-2	CD/HPGE	pn/po	hbl harzburgite		14.3		85.7							merenskyite
RHP01-078-3-1	CD/HPGE	cp	hbl harzburgite	29.0			71.0							moncheite
RHP01-078-4	CD/HPGE	Ag-pn/po	hbl harzburgite	28.3	9.9		61.8							moncheite
RHP01-078-5	CD/HPGE	cp	hbl harzburgite	17.1	9.4		65.9	7.6						moncheite
RHP01-078-6	CD/HPGE	pn	hbl harzburgite	19.7	12.7		67.6							moncheite
RHP01-078-7	CD/HPGE	cp	hbl harzburgite	9.8			63.7	26.6						moncheite
RHP01-078-8	CD/HPGE	cp/pn	hbl harzburgite	14.0	12.9		73.1							moncheite

Table 1. cont'd.

RHP01-078-9-1	CD/HPGE	pn/sil	hbl harzburgite				36.8	63.2				hessite
RHP01-078-9-2	CD/HPGE	pn/sil	hbl harzburgite	10.9	11.3		57.1	16.8				moncheite
RHP01-078-10	CD/HPGE	cp	hbl harzburgite		14.2		71.7	14.1				merenskyite
RHP01-078-11	CD/HPGE	pn/cp	hbl harzburgite	18.3	13.5		68.3					moncheite
RHP01-078-12	CD/HPGE	cp	hbl harzburgite	28.4	9.7		61.9					moncheite
<u>1600 orebody</u>												
179-E-410-1-1	CD/HPGE	pn	lherzolite		10.9	7.8	81.4					merenskyite
179-E-410-5-1	CD/HPGE	po	lherzolite		5.1	4.1	90.7					unknown
179-E-410-5-2	CD/HPGE	po	lherzolite		3.2	26.7	70.1					merenskyite
179-E-410-5-3	CD/HPGE	pn	lherzolite		4.7	8.4	86.9					unknown
179-E-410-5-4	CD/HPGE	pn	lherzolite		3.4	40.2	56.4					tellurobismuthite
179-E-410-6-1	CD/HPGE	pn	lherzolite		5.3	5.5	89.2					unknown
179-E-410-12-1	CD/HPGE	pn	lherzolite		3.3	23.3	73.4					merenskyite
179-E-410-13-1	CD/HPGE	pn/po	lherzolite		4.8	29.5	65.7					tellurobismuthite
179-E-410-14-1	CD/HPGE	po	lherzolite		1.7	40.1	58.1					tellurobismuthite
179-E-410-15-1	CD/HPGE	po	lherzolite		6.6	46.7	46.7					tellurobismuthite
<u>4600 orebody</u>												
M29-21-3-1	NT/SM	pn	harzburgite		2.0		98.0					tellurium
M29-21-6-1	NT/SM	pn/po	harzburgite		3.4		96.6					tellurium
M29-21-9-1	NT/SM	pn/po	harzburgite		2.8		97.2					tellurium
M29-21-12-1	NT/SM	pn	harzburgite		1.5		98.5					tellurium
<u>Mill Site Dump</u>												
RHP01-109-2-1	D	cp	orthopyroxenite			87.1			10.6	2.2		parkerite
RHP01-109-2-2	D	cp	orthopyroxenite			87.1			10.6	2.2		parkerite
RHP01-109-2-3	D	cp	orthopyroxenite				44.3	55.7				hessite
RHP01-109-2-4	D	cp	orthopyroxenite				44.3	55.7				hessite
RHP01-109-3-1	D	cp	orthopyroxenite				26.2				73.8	altaite
RHP01-109-6-1	D	cp	orthopyroxenite				41.7	58.3				hessite
RHP01-109-6-3	D	cp/cub	orthopyroxenite					20.0			80.0	altaite
RHP01-109-6-5	D	cub	orthopyroxenite				45.6	54.4				hessite
RHP01-109-6-6	D	cp	orthopyroxenite				26.8	6.2			67.0	altaite
RHP01-109-6-7	D	cp	orthopyroxenite				23.3				76.7	altaite
RHP01-109-7-1	D	cp/nc	orthopyroxenite				27.9				72.1	altaite
RHP01-109-8-1	D	cp/sil	orthopyroxenite		11.7	88.3						froodite
RHP01-109-8-2	D	sil	orthopyroxenite			90.1	9.9					hedleyite

Table 1. cont'd.

Climax orebody											
71-EI-615A-1	NT	pn/cp/sil	websterite	16.9		83.1					merenskyite
71-EI-615A-2	NT	pn	websterite	16.9		83.1					merenskyite
71-EI-615A-3	NT	pn/cp	websterite	23.9		76.1					merenskyite
71-EI-615A-4	NT	pn	websterite	21.1		78.9					merenskyite
71-EI-615A-5	NT	po	websterite	16.8	10.1	66.0	7.2				Ni-merenskyite
71-EI-615A-6-1	NT	pn	websterite	26.4	11.9	61.8					merenskyite
71-EI-615A-6-2	NT	cp	websterite	26.4	11.9	61.8					merenskyite
71-EI-615A-7-1	NT	pn/cp/sil	websterite	17.8	6.0	69.2	7.1				Ni-merenskyite
71-EI-615A-7-2	NT	cp	websterite	17.8	6.0	69.2	7.1				Ni-merenskyite
71-EI-615A-7-3	NT	cp/mer	websterite					22.4	36.7	40.8	hollingworthite
71-EI-615A-8	NT	pn	websterite	23.1		76.9					merenskyite
71-EI-615A-9	NT	cp/sil	websterite	22.3		77.7					merenskyite
71-EI-615A-10	NT	pn	websterite	13.4		86.6					merenskyite
71-EI-615A-11	NT	pn/sil	websterite	15.1		84.9					merenskyite

[1]NT= Net-textured sulphide, SM = semi-massive sulphide, CD = coarse disseminated sulphide, D = disseminated sulphide, HPGE = high-PGE mineralization (> 1.5 ppm total PGE). [2]po = pyrrhotite, pn = pentlandite, cp = chalcopyrite, cub = cubanite, py = pyrite, nc = nickeline, mer = merenskyite, sil = silicate mineral. [3]ol = olivine, hbl = hornblende.

Table 2. Electron-microprobe analyses of platinum-group and precious-metal minerals from the Giant Mascot Ni-Cu-PGE deposit. Raw X-ray data converted to wt.% by the Cameca PAP matrix correction program (Carlton University, Ottawa).

Sample	Mineralization[1]	Host mineral[2]	Host rock[3]	Pt	Pd	Bi	Te	Ag	Ni	S	As	Sb	Mineral Name
3550 East Portal Dump													
RHP01-152-43	NT/HPGE	po	ol websterite	14.8	7.5	8.2	62.0		5.7			0.5	Pd-moncheite
RHP01-152-47	NT/HPGE	py	ol websterite	15.0	12.5	7.8	59.5		2.7			0.5	Pt-merenskyite
RHP01-152-52	NT/HPGE	cp	ol websterite	28.6	0.5	0.1	0.2			23.5	36.2		sperrylite
RHP01-152-57	NT/HPGE	py/cp	ol websterite	22.0	10.6	5.5	60.6		1.3			0.5	Pd-moncheite
RHP01-152-58	NT/HPGE	py/cp	ol websterite	15.3	11.9	6.2	61.7		3.1			0.5	Pt-merenskyite
RHP01-152-59	NT/HPGE	pn	ol websterite	15.1	6.6	7.6	57.6	0.7	5.4	0.1		0.5	Pd-moncheite
RHP01-109-88	D	cp	orthopyroxenite			62.8			27.0	10.1		0.8	parkerite
12MMA-5-8-5A-71	CD	tr	lherzolite		11.0	12.0	64.9		10.6			0.5	Pd-melonite
12MMA-5-8-5A-75	CD	po	lherzolite		10.9	11.9	65.2		10.8			0.4	Pd-melonite
12MMA-5-8-5A-76	CD	po	lherzolite		1.7	1.3	39.3	53.8	1.6			0.5	hessite
12MMA-5-8-5A-81	CD	pn	lherzolite		4.4	11.5	67.4		15.7			0.5	Pd-melonite
12MMA-5-8-5A-83	CD	pn	lherzolite		2.6	9.1	68.4		16.8			0.5	Pd-melonite
12MMA-5-8-5A-84	CD	pn	lherzolite		10.6	12.3	64.4		11.3			0.5	Pd-melonite
12MMA-5-8-5A-91	CD	po/tr	lherzolite		9.0	8.5	65.9		11.9	4.1		0.3	Ni-merenskyite
12MMA-5-8-5A-92	CD		lherzolite		9.4	11.6	66.5		12.1			0.6	Pd-melonite
4600 orebody													
M29-21-69	NT/SM	pn	harzburgite	0.1	1.4	0.1	77.2		19.4			0.2	Pd-melonite
M29-21-71	NT/SM	pn	harzburgite	0.1	1.9		70.2		22.9	4.1		0.1	Pd-melonite
Chinaman orebody													
71-EI-632-60	CD	pn	orthopyroxenite				37.8	61.0	0.9	0.4		0.2	hessite
71-EI-632-64	CD	pn	orthopyroxenite		4.9	0.8	79.4		16.0			0.6	Pd-melonite
71-EI-632-68	CD	pn	orthopyroxenite				35.4	61.4		0.4		0.2	hessite
71-E1-657-23	NT	po/pn	hbl orthopyroxenite	55.1					0.1	0.9	43.0		sperrylite
Climax orebody													
71-EI-615A-23	NT	cp	websterite		19.5	5.7	59.6		7.0	3.3		0.2	merenskyite
71-EI-615A-31	NT	pn/cp	websterite		18.0	9.5	65.5		6.8	0.2		0.5	Ni-merenskyite
1600 orebody													
179-E-847-65	SM/HPGE	pn/po	hbl lherzolite	2.0	10.9	7.7	67.0		10.4			0.5	Pd-melonite
179-E-847-66	SM/HPGE	cp	hbl lherzolite		19.5	13.3	58.1		4.1			0.5	merenskyite
179-E-410-42	CD/HPGE	po	lherzolite		10.5	9.4	68.5		10.3			0.5	Pd-melonite
179-E-410-51	CD/HPGE	po	lherzolite	0.3	12.6	12.5	63.1		8.8	0.3		0.4	Ni-merenskyite

[1]NT= Net-textured sulphide, SM = semi-massive sulphide, CD = coarse disseminated sulphide, D = disseminated sulphide, HPGE = high-PGE mineralization (> 1.5 ppm total PGE). [2]po = pyrrhotite, pn = pentlandite, cp = chalcopyrite, py = pyrite, tr = troilite. [3]ol = olivine, hbl = hornblende.

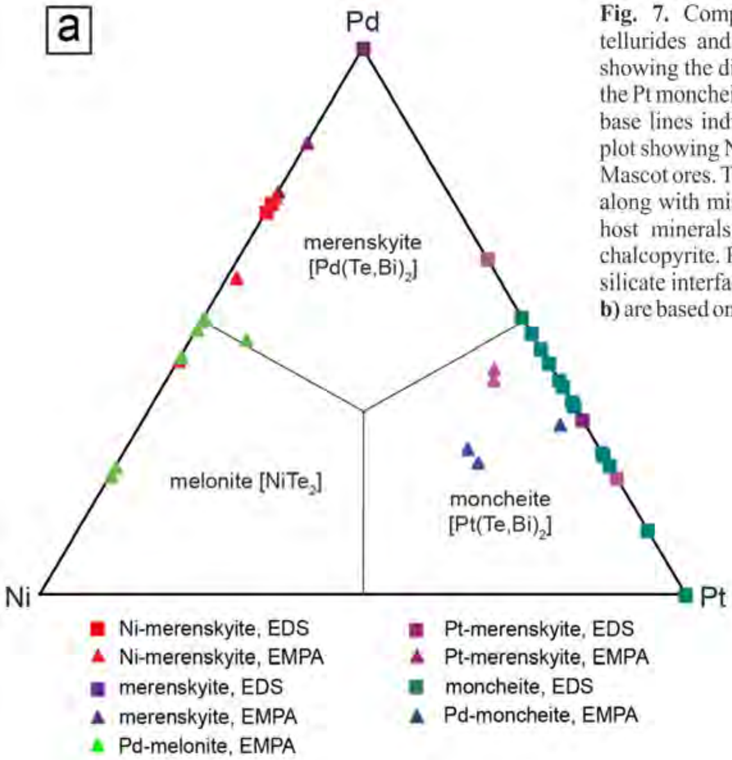

Fig. 7. Compositions of platinum, palladium, and nickel-bearing tellurides and their host minerals at Giant Mascot. **a)** Ternary plot showing the distribution of telluride and bismuthotelluride varieties for the Pt moncheite, Pd merenskyite, and Ni melonite end-members, where base lines indicate solid-solution series between minerals. **b)** Ternary plot showing Ni+Pd+Pt, Te and Bi for platinum-group minerals in Giant Mascot ores. The most common PGM are tellurides containing Pd and Pt along with minor Bi and Ni. **c)** Histogram showing the most common host minerals for PGM, predominantly pentlandite, pyrrhotite and chalcopyrite. PGM are fully enclosed, at sulphide-sulphide or sulphide-silicate interfaces, or in fracture fillings. Analyses plotted in Figs **a)** and **b)** are based on 100% normalized EDS and EMPA results.

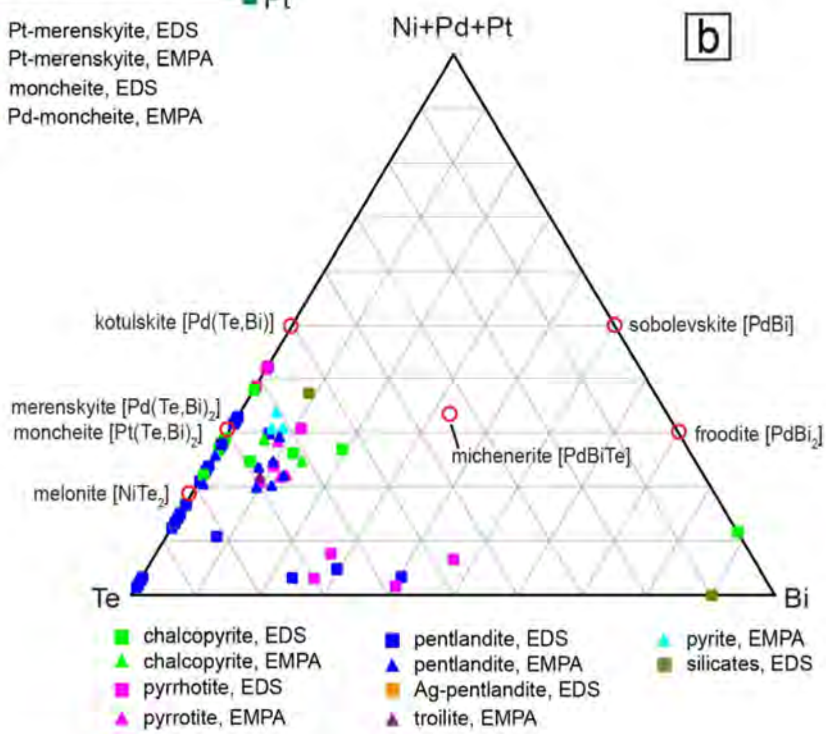

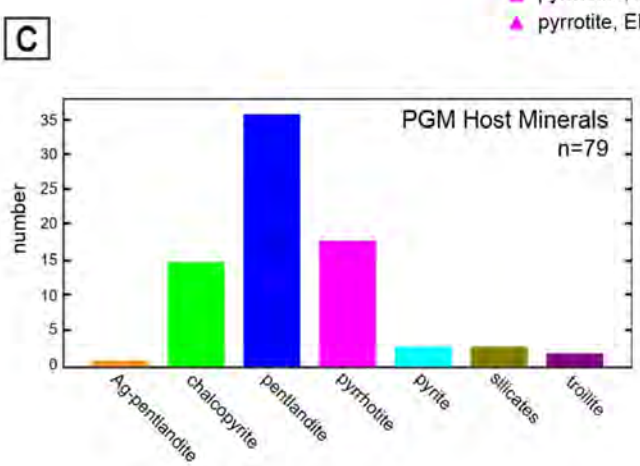

1988a; Helmy, 2004). The limited substitution of Sb and Bi for Te in PGM is further evidence for an orthomagmatic origin (e.g., Helmy, 2005).

The textures of sulphide minerals in the Giant Mascot intrusion reveal a multistage evolution of the primary magmatic sulphide melt during cooling and subsequent crystallization. Strained and fractured sulphide and silicate minerals appear consistent with significant subsolidus compaction during the formation of the ores and cumulate sequences. Late-stage magmatic remobilization involving iss and residual semimetal-rich melts resulted in the formation of chalcopyrite veins. Low-temperature minerals, such as troilite, violarite and mackinawite, indicate significant subsolidus reequilibration of the sulphides during cooling.

9. Current and future research

Ongoing research on the Giant Mascot Ni-Cu-PGE deposit and ultramafic-mafic intrusion aims to develop a paragenetic history of the ultramafic suite and associated sulphides and PGM. Whole-rock PGE and trace element geochemistry is being used to investigate the petrogenesis of the Giant Mascot ultramafic-mafic intrusion. U-Pb and $^{40}Ar/^{39}Ar$ geochronology is being conducted to define age relationships and tectonic setting and increase our knowledge of the formation and processes for orogenic Ni-Cu-PGE ore systems. Sulphur isotope analyses of sulphide minerals in the ultramafic and mafic rocks and Settler schist, combined with electron-probe microanalysis of the nickel contents in olivine, aim to identify a mechanisms for sulphide saturation of the Giant Mascot parental magma(s) and formation of associated Ni-Cu-PGE mineralization.

10. Conclusions

This study reports the first platinum-group minerals identified in the Giant Mascot Ni-Cu-PGE deposit.

1) Platinum-group minerals commonly occur as Pd-, Pt- and Ni-bismuthotellurides hosted by base-metal sulphides, predominantly pentlandite.
2) Textures of sulphides and platinum-group minerals indicate an orthomagmatic origin involving exsolution from base-metal sulphides.
3) Textures of precious-metal minerals indicate late-stage crystallization from residual melts rich in base and precious metals.
4) The predominance of Te-bearing PGM and PMM associated with sulphides indicates a high Te concentration of the parental magma, either derived from the mantle source or assimilated during transport through mid-crustal levels.
5) PGE-enriched sulphides containing identifiable platinum-group minerals in the Giant Mascot intrusion indicate that orogenic Ni-Cu mineralization in the Canadian Cordillera and elsewhere may provide significant targets for economic Ni-Cu-PGE deposits.

Acknowledgments

We thank Dr. Mati Raudsepp, Jenny Lai, Elisabetta Pani, and Edith Czech (UBC), and Patricia Hunt (GSC-Ottawa) for SEM advice and training, and Dr. Ingrid Kjarsgaard for microprobe analytical work on PGM. A tremendous thanks to Corey Wall, Wes Harmon, Alex Colyer, and Lauren Harrison for help with fieldwork in 2012-2013. We also thank Valley Helicopters in Hope for flights to Giant Mascot, and Barrick Gold and Fraser Valley Dirt Riders Association for access to their property. Dr. Jon Scoates and Dr. Michel Houlé generously provided a thorough review of the manuscript at short notice. Editorial comments by Dr. Lawrence Aspler helped improve the manuscript. Funding for this project is provided by Natural Resources Canada through the Geological Survey of Canada's Targeted Geoscience Initiative 4 (TGI-4: 2011-2015) Magmatic-Hydrothermal Nickel-Copper-PGE-Chrome Ore System Project. Additional funding was provided by a SEG Canadian Foundation Graduate Student Research Grant awarded to Matthew Manor in 2013. This is Earth Sciences Sector contribution number 20130343.

References cited

Afifi, A.M., Kelly, C.K., Essene, E.J., 1988a. Phase relations among tellurides, sulphides, and oxides. In: Thermochemical data and calculated equilibria. Economic Geology, 83, 377-395.

Aho, A.E., 1954. Geology and ore deposits of the property of Pacific Nickel Mines near Hope, British Columbia. Unpublished Ph.D. Thesis, University of California Santa Barbara, 158 p.

Aho, A.E., 1956. Geology and genesis of ultrabasic nickel-copper-pyrrhotite deposits at the Pacific Nickel Property, southwestern British Columbia. Economic Geology, 51, 441-481.

Barkov, A.Y., Laflamme, J.H.G., Cabri, L.J., and Martin, R.F., 2002. Platinum-group minerals from the Wellgreen Ni-Cu-PGE deposit, Yukon, Canada. Canadian Mineralogist, 40, 651-669.

Becker, M., de Villiers, J., and Bradshaw, D., 2010. The mineralogy and crystallography of pyrrhotite from selected nickel and PGE ore deposits. Economic Geology, 105, 1025-1037.

Brown, E.H., and McClellan, W.C., 2000. Pluton emplacement by sheeting and vertical ballooning in part of the southeast Coast Plutonic Complex, British Columbia. Geological Society of America Bulletin, 1125, 708-719.

Cabri, L.J., and Laflamme, J.H.G., 1976. The mineralogy of the platinum-group elements from some copper–nickel deposits of the Sudbury area, Ontario. Economic Geology, 71, 1159-1195.

Christopher, P.A., and Robinson, J.W., 1974. Pride of Emory Mine 92H/SW-4. Exploration and Mining in British Columbia 1974, British Columbia Department of Mines and Petroleum Resources, 105-113.

Greene, A.R., Scoates, J.S., Weis, D., and Israel, D., 2009. Geochemistry of Triassic flood basalts from the Yukon (Canada) segment of the accreted Wrangellia oceanic plateau. Lithos, 110, 1-19.

Helmy, H.M., 2004. Cu–Ni–PGE mineralization in the Genina Gharbia mafic–ultramafic intrusion, Eastern Desert, Egypt. Canadian Mineralogist, 42, 351-370.

Helmy, H.A., 2005. Melonite group minerals and other tellurides from three Cu-Ni-PGE prospects, Eastern Desert, Egypt. Ore Geology Reviews, 26, 305-324.

Holwell, D.A., and McDonald, I., 2010. A review of the behaviour of platinum group elements within natural magmatic sulphide ore systems. Platinum Metals Review, 541, 26-36.

Hulbert, L.J., 2001. GIS maps and databases of mafic-ultramafic hosted Ni, Ni-Cu, Cr +/- PGE occurrences and mafic-ultramafic bodies in British Columbia. British Columbia Ministry of Energy and Mines, Geoscience Map 2001-2.

McLeod, J.A., 1975. The Giant Mascot ultramafite and its related ores. Unpublished M.Sc. Thesis, University of British Columbia, 136 p.

Metcalfe, P., McClaren, M., Gabites, J.E., and Houle, J., 2002. Ni-Cu-PGE deposits in the Pacific Nickel Complex, southwestern BC; a profile for magmatic Ni-Cu-PGE mineralization in a transpressional magmatic arc. Exploration and Mining in British Columbia, Ministry of Energy, Mines and Petroleum Resources, pp. 65-80.

Mitrovic, I., 2013. Evolution of the Coast Cascade orogen by tectonic thickening and magmatic loading: the Cretaceous Breakenridge Complex, southwestern British Columbia. Unpublished M.Sc. Thesis, Simon Fraser University, 133 p.

Mota-e-Silva, J., Ferreira Filho, C.F., Bühn, B., and Dantas, E.L., 2011. Geology, petrology and geochemistry of the "Americano do Brasil" layered intrusion, central Brazil, and its Ni-Cu sulphide deposits. Mineralium Deposita, 46, 57-90.

Mota-e-Silva, J., Ferreira Filho, C.F., and Della Giustina, M.E.S., 2013. The Limoeiro deposit: Ni-Cu-PGE sulphide mineralization hosted within an ultramafic tubular magma conduit in the Borborema Province, northeastern Brazil. Economic Geology, 108, 1753-1771.

Muir, J.E., 1971. A preliminary study of the petrology and ore genesis of the Giant Mascot 4600 ore body, Hope, British Columbia. Unpublished M.Sc. Thesis, University of Toronto, 125 p.

Naldrett, A.J., 2004. Magmatic sulphide deposits: geology, geochemistry and exploration. Springer, Berlin, 727 p.

Nixon, G.T., Hanmack, J.L., Ash, C.H., Cabri, L.J., Case, G., Connelly, J.N., Heanmn, L.M., LaFlamme J.H.G., Nuttall, C., Paterson, W.P.E., and Wang, R.H., 1997. Geology and platinum-group-element mineralization of Alaskan-type ultramafic-mafic complexes in British Columbia. British Columbia Ministry of Employment and Investment, British Columbia Geological Survey Bulletin 93, 142 p.

Nixon, G.T., 2003. Use of spinel in mineral exploration: the enigmatic Giant Mascot Ni-Cu-PGE deposit - possible ties to Wrangellia and metallogenic significance. In: Geological Fieldwork 2002, British Columbia Ministry of Energy, Mines and Petroleum Resources, British Columbia Geological Survey Paper 2003-1, pp. 115-128.

Paktunc, A.D., 1989. Petrology of the St. Stephen Intrusion and the genesis of related nickel-copper sulphide deposits. Economic Geology, 84, 817-840.

Pigage, L.C., 1973. Metamorphism southwest of Yale, British Columbia. Unpublished M.Sc. Thesis, University of British Columbia, 114 p.

Piña, R., Gervilla, F., Ortega, L., and Lunar, R., 2008. Mineralogy and geochemistry of platinum-group elements in the Aguablanca Ni-Cu deposit (SW Spain). Mineralogy and Petrology, 92, 259-282.

Pinsent, R.H., 2002. Ni-Cu-PGE potential of the Giant Mascot and Cogburn ultramafic-mafic bodies, Harrison-Hope area, southwestern British Columbia 092H. In: Geological Fieldwork 2001, British Columbia Ministry of Energy, Mines and Petroleum Resources, British Columbia Geological Survey Paper 2002-1, pp. 211-236.

Reiners, P.W., Ehlers, T.A., Garver, J.I., Mitchell, S-G., Montgomery, D.R., Vance, J.A., and Nicolescu, S., 2002. Late Miocene exhumation and uplift of the Washington Cascade Range. Geology, 309, 767-770.

Richards, T.A., 1971. Plutonic rocks between Hope, B.C. and the 49th Parallel. Unpublished Ph.D. Thesis, University of British Columbia, 193 p.

Richards, T.A., and McTaggart, K.C., 1976. Granitic rocks of the southern Coast Plutonic Complex and northern Cascades of British Columbia. Geological Society of America Bulletin, 87, 935-953.

Ripley, E.M., 2010. Chapter 24 - A new perspective on exploration for magmatic sulphide-rich Ni-Cu-PGE deposits. Economic Geology Special Publication, 15, 437-450.

Sappin, A.A., Constantin, M., and Clark, T., 2012. Petrology of mafic and ultramafic intrusions from the Portneuf-Mauricie Domain, Grenville Province, Canada: implications for plutonic complexes in a Proterozoic island arc. Lithos, 154, 277-295.

Stephens, F.H., 1959. New nickel production in British Columbia. Western Miner and Oil Review (August), 28-33.

Vining, M.R., 1977. The Spuzzum pluton northwest of Hope, B.C. Unpublished M.Sc. Thesis, University of British Columbia, 159 p.